Electronic supplementary materials *Mendeleev Commun.*, 2020, **30**, 288-290

Energy of the surface segregation of Ag atoms in Ag–Au alloys in an aqueous solution

Sergey V. Doronin

S1. Experimental procedure

Segregation in the Ag–Au alloy and coverage of the Au electrode with the Ag deposits were performed in a three-electrode electrochemical cell with common area between a working and an auxiliary electrode using LTJ and CV methods. The electrodes were represented by an end-side of a wire, 0.7 mm in diameter of the 10% Ag–Au alloy (mole fraction for silver is given), which is pasted into a glass capillary. The electrodes were polished with the Al_2O_3 powder, 0.3 μm in diameter.

The solutions were deaerated with argon gas passed through a column which was filled with activated carbon.

Electrochemical measurements were carried out using an Elins-P30I potentiostat. Background electrolyte (0.1 M NaF) was additionally cleaned in a quartz cell by ultraviolet irradiation (λ = 253.7 nm).

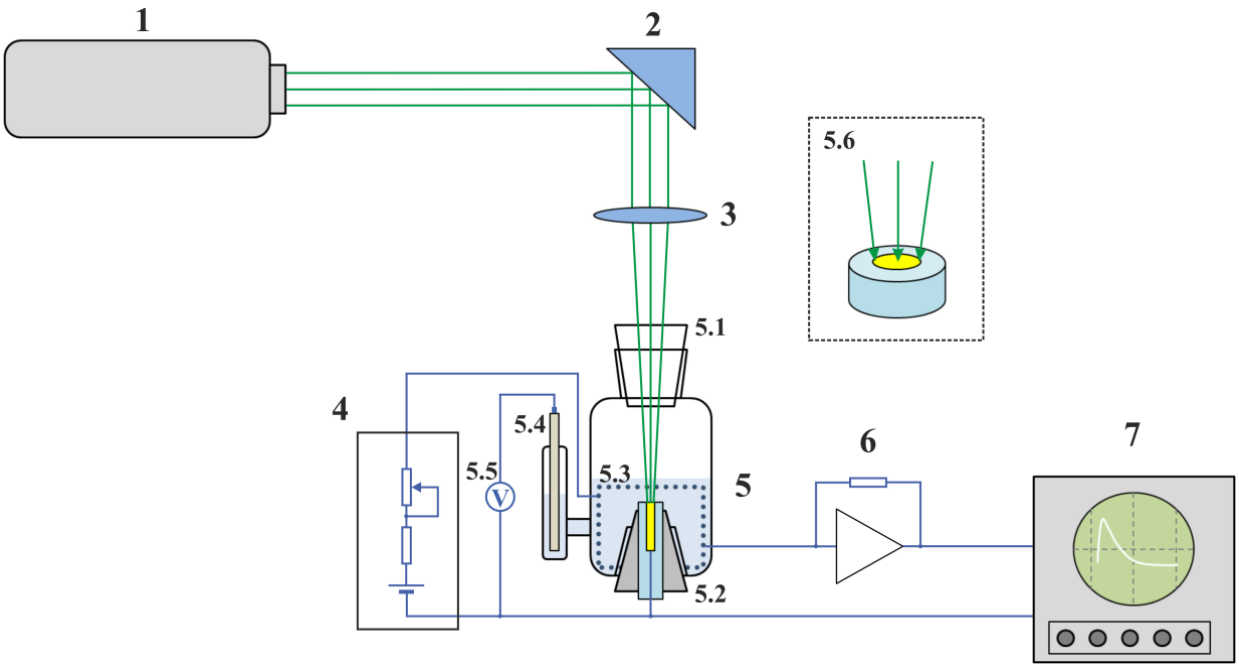

Figure S1 Schematic representation of the experimental set up used for laser temperature jump measurement. Legend: **1** is a solid-state laser; **2** is a mirror; **3** is a lens to focus irradiation at an electrode surface; **4** is a potentiostating system for the working electrode; **5** is an electrochemical cell; **5.1** is an optical window; **5.2** is a working electrode pasted into a fluoroplastic joint; **5.3** is an auxiliary electrode as a Pt mesh cylinder; **5.4** is a saturated calomel reference electrode; **5.5** is a digital voltmeter; **5.6** is a schematic relation of the electrode diameter and the focused laser irradiation; **6** is a differential current feedback amplifier (amplification coefficient is ~ 80); **7** is a digital oscillograph.

The LTJ measurements were performed in a three-electrode electrochemical cell, the working electrode was irradiated with the laser at varied potential. Figure S1 shows the experimental set up that was equipped with the DTL-394QT solid-state laser with the wavelength of 527 nm and pulse duration of 8 ns. Induced potential jump ΔE_{TJ} was recorded with a digital LA-n10M4 oscillograph, and the ΔE_{TJ} value was obtained as function of the potential of the working electrode. In order to reduce noise, the TJ signal was averaged over *ca.* 200–500 pulses, the electrochemical cell and the amplifier were screened with a particular care, and the laser was placed in a separate screened room.

The coverage density of the electrode θ_{Ag} was found from an approximation of the experimental LTJ data (ΔE_{TJ}) with the equation used: $\Delta E_{TJ} = \theta_{Ag} \times \Delta E_{TJ,Ag} + (1 - \theta_{Ag}) \times \Delta E_{TJ,Au}$, where $\Delta E_{TJ,Au}$ are the signals of the temperature jump on the pure silver and golden surfaces.

S2. Details of the DFT calculations

The quantum-chemical calculations were performed in the Quantum ESPRESSO software[S1] within the framework of generalized gradient approximation by the PBE functional[S2] according to the Vanderbilt ultrasoft pseudopotential.[S3] According to the previous works,[S4–S6] this functional may be successfully applied to describe the water–metal boundary. Maximum energy level was taken as 475 eV and smearing σ = 0.14 eV. To integrate over the Brillouin zone, the method of special points of Monkhorts-Pack[S7] with the *k*-point mesh of 5×5×1 was applied. The (100) and (111) faces were presented by the clusters consisting of 40 and 45 metal atoms that is equivalent to 5 atomic layers. Distance between the cluster planes was 15 Å. Geometry of all molecules and atoms of the metal cluster added onto the surface was optimized.

The DFT calculated parameters such as lattice constant, cohesion energy, elasticity modulus, electronic work function and surface tension for Ag and Au are comparable with experimental data (Table S1).

Table S1 Comparison of calculated and experimental parameters, where a_0 is lattice constant, E_{coh} is cohesion energy, B is an elasticity modulus, W is electronic work function, and $\boldsymbol{\gamma}$ is surface tension. The W and $\boldsymbol{\gamma}$ parameters for the (100)/(111) faces are slashed.

Metal	a_0/Å		E_{coh}/eV		B/GPa		W/eV		γ/J m^{-2}	
	calc.	lit.[S8]	calc.	lit.[S9]	calc.	lit.	calc.	lit.	calc.	lit.[S11]
Au	4.085	4.078	3.88	3.93	171.3	173[S10]	5.18 / 5.35	5.47 / 5.31[S8]	1.107 / 0.887	1.627 / 1.28
Ag	4.057	4.086	3.25	2.85	116.5	104[S10]	4.37 / 4.59	4.64 / 4.74[S8]	1.038 / 0.928	1.238 / 1.172

Atom relaxation was performed by the Broyden–Fletcher–Goldfarb–Shanno (BFGS) algorithm, convergence criterion in energy calculations was taken as 10^{-4} eV and maximum force acting on the atoms was 10^{-3} eV/Å. Water, adsorbents and the monolayer of a metal were added from either sides of the cluster to eliminate the dipole moment. Geometry of all molecules and atoms added onto the surface as well as two layers of the substrate metal were optimized.

S3. Calculation of Segregation Energy

Segregation was modeled with the DFT calculations as follows: the silver atom was exposed from the cluster bulk (b) onto the surface (s) (Figure S2), the calculated energies $\Delta E_{seg} = E_s - E_b$ are difference between the energy of the initial and final states.

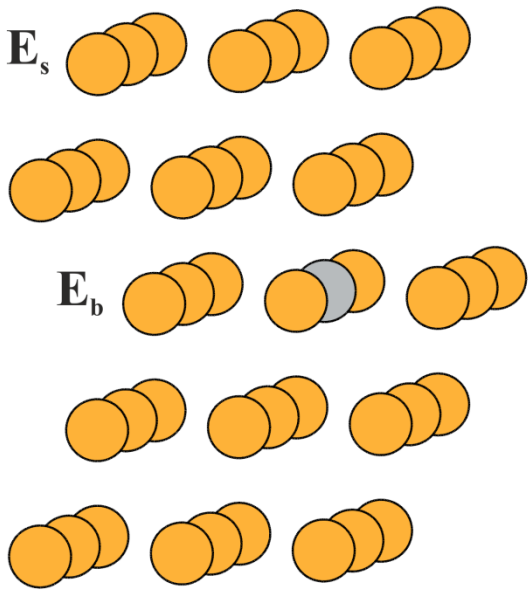

Figure S2 Segregation of silver with the (111) Au cluster with the water monolayer on either side. Silver is exposed from the cluster bulk (b) onto the surface (s).

Calculation of the Ag–Au system with the (111) Au face taken as an example in vacuum showed that the segregation energy of silver is ca. 0.1 eV. Variations of the cluster in size and thickness (from 5 to 7 Au layers) and change in cross-section (from 9 to 16 atoms), transition to LDA, PAW approximations and to other software packages (for example, the same calculations were performed in VASP in the PAW approximation) have no significant effect on this value. Experimental data show that the segregation energy of silver on a polycrystalline surface in vacuum is *ca.* –0.026 eV. To explain these differences, the clusters with large quantity of silver were calculated.

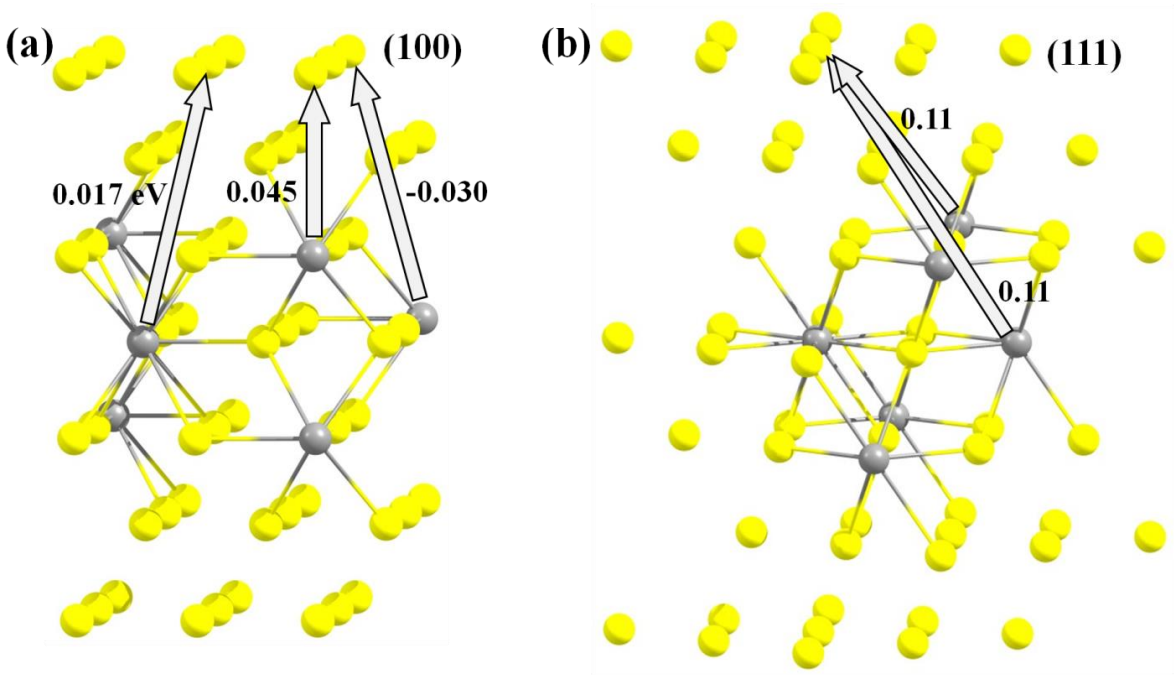

Figure S3 Segregation energy of Ag in the 63-atom cluster modeling the (100) (**a**) and (111) (**b**) faces. Direction of the Ag atom exposition onto the surface is shown by the arrows.

Study of the effect of the cluster composition involved studying the effect of the Ag–Au cluster on the segregation energy of Ag. As the lattice constants of these metals differ from each other, however slightly, the calculations were performed with relaxation of translation period along the cluster plane (the XY plane). The composition varied from 1 to 6 Ag atoms randomly distributed in three central layers of the 63 atom 7-layered cluster of Ag–Au which modeled the relevant face (Figure S3). For 6 Ag atoms, there is the only scenario of the exposition onto the (100) face when ΔE_{seg} was –0.03 eV (Figure S3), for other cases including the (111) face, the energy remained positive that is the process was wasteful.

Use of large clusters with several atoms of silver may change the observed situation in some cases. The only negative here is that the approach with large clusters used significantly increases time of calculations and retards studying the water effect on segregation as it requires to calculate a number of structures equivalent to various scenarios of silver exposition onto the surface.

S4. Adsorption of water and •OH on the segregated atom Ag

Figure S4 depicts the data given in Table 1 from the main part of this manuscript, for visual clarity.

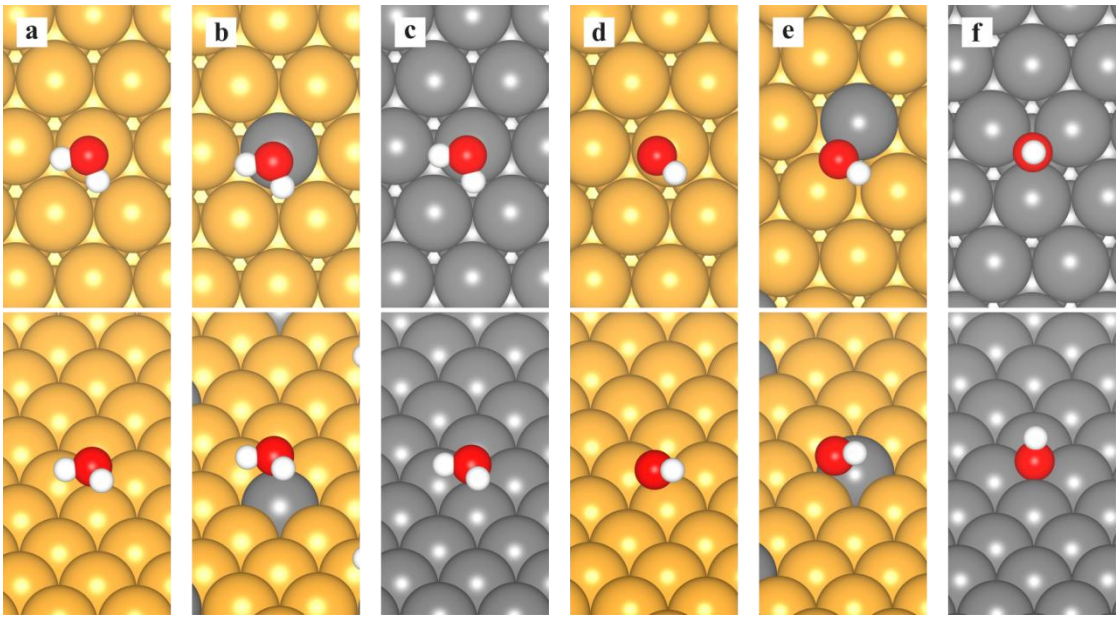

Figure S4 Adsorbed molecule of water (**a–c**) and hydroxyl (**d–f**) on the (111) face of Au, Ag, and on the segregated atom of silver.

S5. Evaluation of absolute values of the surface energy of silver and gold in an electrolyte.

For further analysis, the literature data for Ag and Au were used (Table S2).

Table S2 Physical parameters for Ag and Au. a_0 is lattice constant, γ_{poly} is surface tension for the polycristalline surface with vacuum, γ_{NNN} is surface tension for a corresponding (NNN) face, H_m and H_{vap} are the enthalpies of melting and vaporization.

Parameters	ref.	Au	Ag
a_0/Å	S12	4.0874	4.0857
γ_{poly}/J m^{-2}	S13	1.128	0.923
γ_{111}/J m^{-2}	S11	1.283	1.172
γ_{100}/J m^{-2}	S11	1.627	1.2
γ_{110}/J m^{-2}	S11	1.7	1.238
H_m/kJ mol^{-1}	S13	12.552	11.297
H_{vap}/kJ mol^{-1}	S13	334.4	250.6

Experimental data for the surface energy for the (111) Ag and Au faces in the solution of 0.1 M $HClO_4$ were taken from the work.[S14]

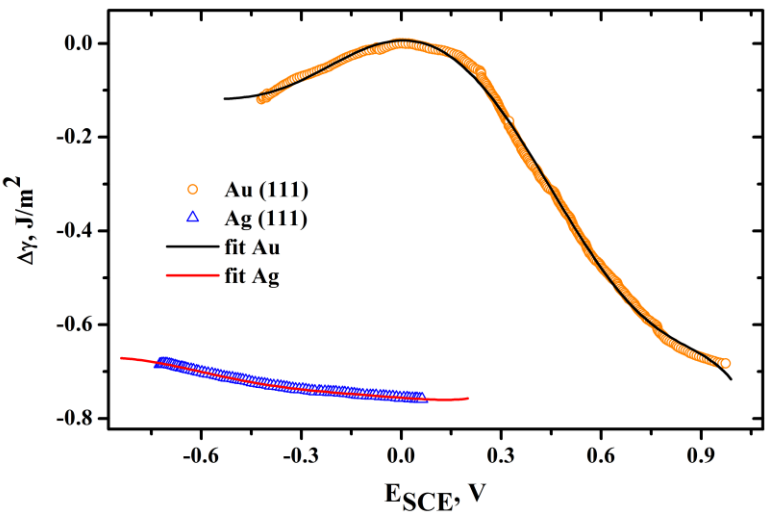

Figure S5 Relative surface energies of the Ag, Au (111) faces as function of the potential in the solution of 0.1 M $HClO_4$.[S14] Experimental data are empty circle, polynomial approximation is lines.

The data [Figure S5] were approximated by polynomials for further convenient transformations:

$\gamma_{Au} = 0.00656 + 0.01778\times E - 1.52658\times E^2 - 1.56193\times E^3 + 2.6743\times E^4 + 1.91536\times E^5 - 2.25119\times E^6$

$\gamma_{Ag} = -0.75593 - 0.05149\times E + 0.04598\times E^2 + 0.41649\times E^3 + 1.69891\times E^4 + 1.98009\times E^5 + 0.67669\times E^6$

The next step was a normalization of the $\Delta\gamma$–E dependencies to show absolute surface energy as function of the γ–E potential. For this purpose, the surface tension change is compared for the Hg, Ga liquid metals in going from vacuum to an aqueous solution. In accordance with literature data (Table S3), the surface tension of these metals decreases by 5–10 % in the aqueous solution (γ_s/γ_{vac}). The main factor to reduce γ is a contact of the solvent molecules with the metal atoms. For Ag and Au, γ may be roughly defined in the solution at the zero point charge (ZPC) with the surface energy considered decreased by 5–10 % in going from vacuum to the aqueous solution. The ZPC area corresponds to maximum surface tension of the surface energy since the interaction energy of the solvent and the metal electrode is minimal.

Table S3 Comparison of the surface tension for mercury and gallium in vacuum (γ_{vac}) and in the aqueous solutions (γ_s). The γ_s values were taken at zero-charge potential. The adsorption energy of water $E_{ads}(H_2O)$ was calculated in a cluster model[S15].

Metal	**Me/Vacuum**	**Me/Solution**		**γ_s/γ_{vac}**	**$E_{ads}(H_2O)$/ eV**
	γ_{vac}/J m^{-2}	**Solution**	**γ_s/J m^{-2}**		
Hg	0.4842[S16] (25 °C)	0.05 M Na_2SO_4	0.4622±0.0002[S18] (25 °C)	~0.95	0.37[S15]
	0.480[S17] (19 °C)				
Ga	0.7237[S19] (25 °C)	$NaClO_4$+$HClO_4$	0.6539[S20] (30 °C)	0.90 – 0.95	0.26[S15]
	0.690[S21] (30 °C)	Na_2SO_4+H_2SO_4	0.6489[S20] (30 °C)		

The adsorption energies of water in Table S3 for Hg, Ga are rather exaggerated as they were obtained in the cluster model. A detailed comparison of adsorption energies of water for Ag, Au shows (Table S4) that E_{ads} calculated in the periodic model (which is more precise) is twice lower than that of the cluster. With consideration for this moment, E_{ads} in the periodic model for Hg, Ga and for Ag, Au would be within the same order of magnitude.

Table S4 The adsorption energy ($E_{ads}(H_2O)$) of water molecule and the metal-oxygen distance ($h_{M–O}$) on the (100) and (111) faces calculated in the periodic (slab) and the cluster model.

Face	$h_{M–O}$/Å	$E_{ads}(H_2O)$, eV	
		Slab	Cluster
Ag(100)	2.5[S22], 2.91[S23]	–0.20[S24]	–0.28[S22], –0.50[S23]
Ag(111)	2.78[S25,S26]	–0.18[S25,S26], –0.2[S27], –0.17[S28]	–
Au(100)	2.6[S22], 2.696[S29]	–0.17[S29]	–0.30[S22]
Au(111)	3.02[S25], 2.67[S30], 2.63[S31], 2.845[S32]	–0.13[S25], –0.11[S30], –0.14[S31], –0.15[S33], –0.11[S32]	–

Further evaluations that γ (Table S3) is reduced for the (111) Ag, Au faces by 5% in the course of transition to the aqueous solution. By multiplication of the γ values (Table S2) for the (111) face by 0.95, the surface energies were obtained for each metal at ZPC and the previously gained Δγ–*E* polynomials were normalized to corresponding values for γ at ZPC (Figure S6).

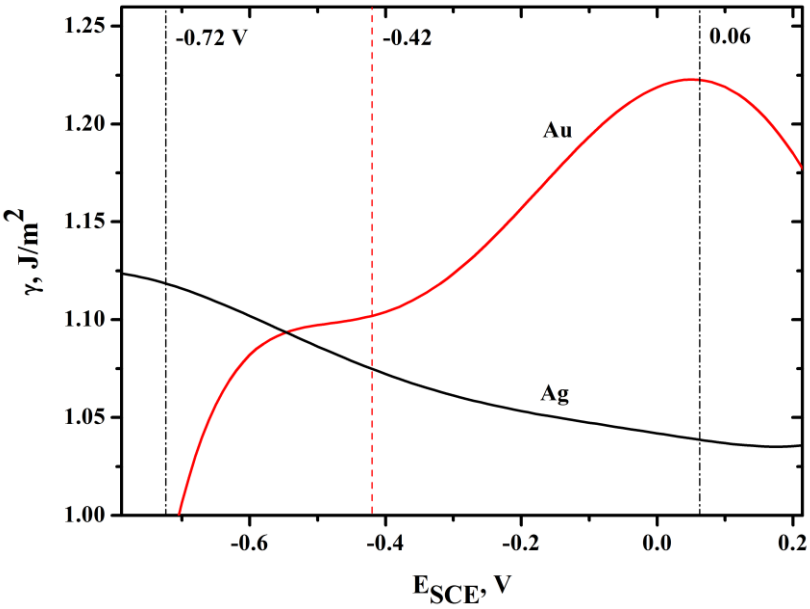

Figure S6 Normalized surface energy obtained by experimental data approximation for the (111) Ag and Au in the solution of 0.1 M $HClO_4$ as function of the electrode potential.[S14] The potential boundaries where experimental data were taken are dotted line for gold and dash dotted line for silver (Figure S5).

S6. Calculation of the segregation energy and surface coverage of silver in various models

One method to calculate the segregation energy is based on calculation of difference between the surface energy for the pure metals[S33] according to the equation

$$\Delta E_{seg} \approx S_{at}\left(\gamma_{Ag}-\gamma_{Au}\right)+\frac{\Delta H_{mix}}{Z\chi(1-\chi)}\left\{Z_Q\left[(1-\theta)^2-\theta^2+\chi^2-(1-\chi)^2\right]+Z_V\left[\chi^2-(1-\chi)^2\right]\right\} \quad \text{(S1)}$$

Where ΔE_{seg} is the surface energy of Ag and Au, S_{at} is an effective square of the segregating atom as the crystal packing for gold and silver does not differ much and is considered the same and equal to 0.4497 m^2 per atom[S34] (the product of $S_{at}\cdot\gamma$ is in eV), θ и χ are the surface coverage by an active component and its mole fraction in the alloy bulk; Z is the coordination number in the alloy bulk, Z_Q is the number of lateral bonds made by an atom within its plane, Z_V is the number of bonds made by an atom to each adjacent plane of atoms, Z_V is number of bonds made by the sought-for atom with an adjacent atomic layer, in particular, for the (111) face $Z = 12$, $Z_Q = 6$, $Z_V = 3$.[S33]

Mixing enthalpy of ΔH_{mix}[S35] in eV for the alloy with silver fraction χ was found by equation as follows:

$$\Delta H_{mix} = \chi(1-\chi)\cdot\left(-16.803-3.233\chi+4.525\chi^2\right)\cdot 1.03641\cdot 10^{-5} \quad \text{(S2)}$$

Surface coverage of silver at given potential E was calculated by equation as follows:

$$\theta=\frac{\frac{\chi}{1-\chi}\exp\left[-\frac{\Delta E_{seg}(E)}{k_B T}\right]}{1+\frac{\chi}{1-\chi}\exp\left[-\frac{\Delta E_{seg}(E)}{k_B T}\right]}, \quad \text{(S3)}$$

where the segregation energy is taken from the equation (S1).

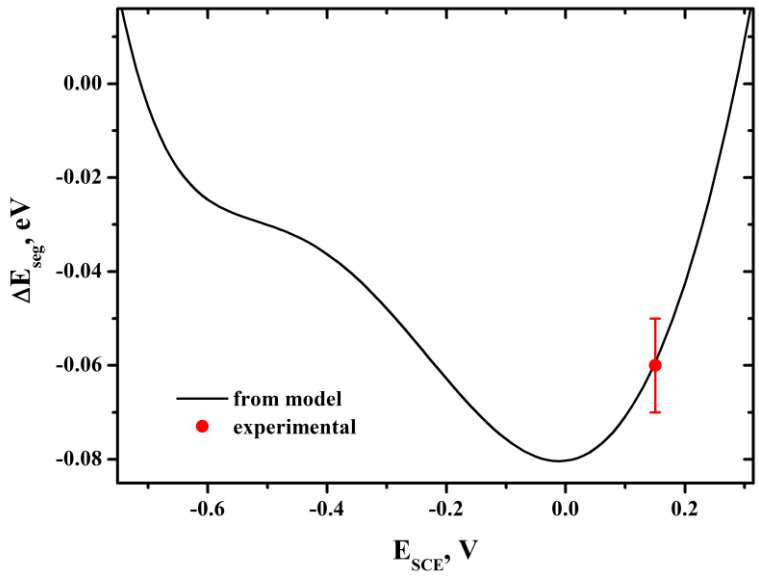

Figure S7 Segregation energy of silver calculated by equations (S1–S3) as function of potential. Experimental data obtained for the 3 and 10 % electrodes are added.

Figure S7 depicts ΔE_{seg} as function of potentials for the Ag–Au system calculated by equations (S1-S3).

The theoretical results were accomplished with the data obtained in[S36,S37] at the mechanically recovered 3% electrode in the acidified solution of 0.05 M NaF with the potential varied (Table S5). The ΔE_{seg} value was calculated by equation as follows:

$$\Delta E_{seg} = -k_B T \ln\left(\frac{\theta}{1-\theta}\cdot\frac{1-\chi}{\chi}\right) \qquad (S4)$$

Table S5 Segregation energy and surface coverage of silver with the E potential varied. Maximum surface coverage occurred during potentiostation which lasted ca. 1.5 hour. ΔE_{seg} is calculated by equation as follows (S4).

E, V	θ_{Ag}	ΔE_{seg}, eV
-0.7	0.35	-0.074
-0.3	0.78	-0.123
0.0	0.89	-0.144

Obviously, mechanical renewal of the electrode surface with a sapphire cutter in[S36,S37] significantly differs from other surface conditioning method and that is the reason why its application causes such high coverage density by silver θ_{Ag} = 0.35 – 0.9 for the 3% electrode.

The coverage of 30±10% and 50±10% for the 3 and 10% electrodes (in this work) corresponds to –0.068±0.013 and –0.056±0.01 eV respectively.

Based on the data for differential capacity [Figure S8(a)] of polycrystalline Ag and Au in 0.05 M NaF[S36,S37], *via* integration of C_{diff}–E, the dependence of σ–E was obtained [Figure S8(*b*)].

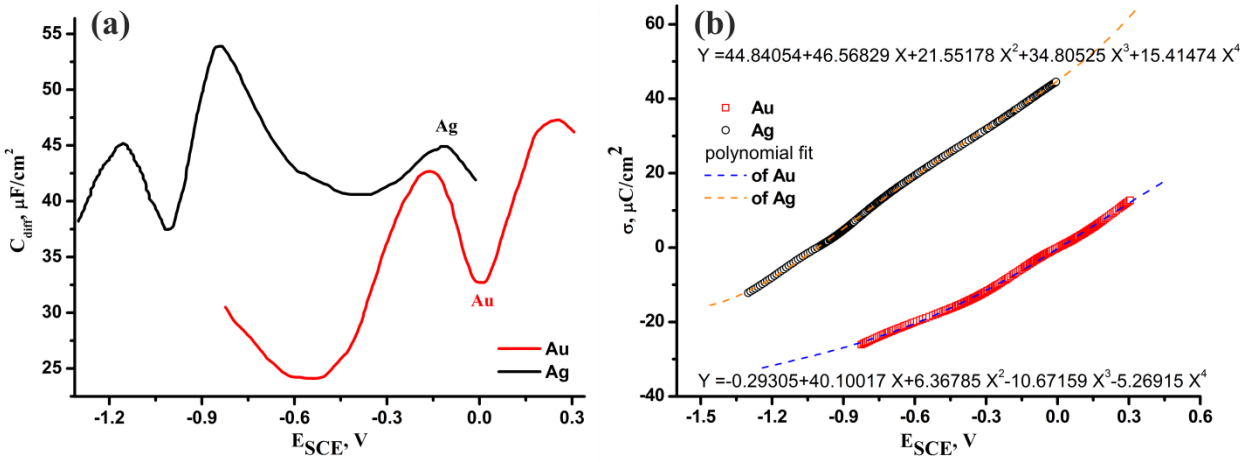

Figure S8 (*a*) Differential capacity[S36] of polycrystalline Ag and Au in 0.05 M NaF and (*b*) Calculated charge densities as function of the potential.

Charge density of the electrodes with the 30±10 % and 50±10 % coverage was calculated with consideration that the total charge on the electrode (σ_θ) at the surface fraction of silver θ is an additive sum (in accordance with the solid layer model suggested in[S36,S37]) of the charge density on the Au and Ag electrodes.

$$\sigma_\theta(E) \approx \theta\cdot\sigma_{Ag}(E) + (1-\theta)\cdot\sigma_{Au}(E) \qquad (S5)$$

References

S1. P. Giannozzi, S. Baroni, N. Bonini, M. Calandra, R. Car, C. Cavazzoni, D. Ceresoli, G. L. Chiarotti, M. Cococcioni, I. Dabo, A. Dal Corso, S. de Gironcoli, S. Fabris, G. Fratesi, R. Gebauer, U. Gerstmann, C. Gougoussis, A. Kokalj, M. Lazzeri, L. Martin-Samos, N. Marzari, F. Mauri, R. Mazzarello, S. Paolini, A. Pasquarello, L. Paulatto, C. Sbraccia, S. Scandolo, G. Sclauzero, A. P. Seitsonen, A. Smogunov, P. Umari and R. M. Wentzcovitch, *J. Phys. Condens. Matter*, 2009, **21**, 395502.

S2. J. P. Perdew, A. Ruzsinsky, G. I. Csonka, O. A. Vydrov, G. E. Scuseria, L. A. Constantin, X. Zhou and K. Burke, *Phys. Rev. Lett.*, 2008, **100**, 13640

S3. D. Vanderbilt, *Phys. Rev. B*, 1990, **41**, 7892.

S4. P. Vassilev, C. Hartnig, M. T. M. Koper, F. Frechard and R. A. van Santen, *J. Chem. Phys.*, 2001, **115**, 9815.

S5. J. VandeVondele, F. Mohamed, M. Krack, J. Hutter, M. Sprik and M. Parrinello, *J. Chem. Phys.*, 2005, **122**, 014515.

S6. B. Santra, A. Michaelides, M. Fuchs, A. Tkatchenko, C. Filippi and M. J. Scheffler, *J. Chem. Phys.*, 2008, **129**, 194111.

S7. M. Methfessel and A. T. Paxton, *Phys. Rev. B*, 1989, **40**, 3616.

S8. *CRC Handbook of Chemistry and Physics*, ed. D. R. Lide, CRC Press, Boca Raton, FL, 2005.

S9. *Metal Reference Book*, 5th edn., ed. C. J. Smithells, Butterworths-Heinemann, London, 1976.

S10. J. R. Neighbours and G. A. Alers, *Phys. Rev.*, 1958, **111**, 707.

S11. L. Vitos, A. V. Ruban, H. L. Skriver and J. Kollár, *Surf. Sci.*, 1998, **411**, 186.

S12. V. A. Lubarda, *Mech. Mater.*, 2003, **35**, 53.

S13. *Handbook of Condensed Matter and Materials Data*, eds. W. Martienssen and H. Warlimont, Springer, Heidelberg, 2005.

S14. C. Friesen, N. Dimitrov, R. C. Cammarata and K. Sieradzki, *Langmuir*, 2001, **17**, 807.

S15. V. Ivaništšev, R. R. Nazmutdinov and E. Lust, *Surf. Sci.*, 2013, **609**, 91.

S16. C. Kemball, *Trans. Faraday Soc.*, 1946, **42**, 526.

S17. R. C. L. Bosworth, *Trans. Faraday Soc.*, 1938, **34**, 1501.

S18. C. A. Smolders and E. M. Duyvis, *Recl. Trav. Chim. Pays-Bas*, 1961, **80**, 635.

S19. G. J. Abbaschian, *J. Less-Common Met.*, 1975, **40**, 329.

S20. A. Frumkin, N. Polianovskaya, N. Grigoryev and I. Bagotskaya, *Electrochim. Acta*, 1965, **10**, 793.

S21. S. C. Hardy, *J. Cryst. Growth*, 1985, **71**, 602.

S22. A. Ignaczak and J. A. N. F. Gomes, *J. Electroanal. Chem.*, 1997, **420**, 209.

S23. C. Qin and J. L. Whitten, *J. Phys. Chem. B*, 2005, **109**, 8852.

S24. K. Honkala, A. Hellman and H. Grönbeck, *J. Phys. Chem. C*, 2010, **114**, 7070.

S25. A. Michaelides, V. A. Ranea, P. L. de Andres and D. A. King, *Phys. Rev. Lett.*, 2003, **90**, 216102.

S26. V. A. Ranea, A. Michaelides, R. Ramirez, J.A. Vergés, P. L. de Andres and D. A. King, *Phys. Rev. B*, 2004, **69**, 205411.

S27. C. G. Sanchez, *Surf. Sci.*, 2003, **527**, 1.

S28. H.-Y. Su, M.-M. Yang, X.-H. Bao and W.-X. Li, *J. Phys. Chem. C*, 2008, **112**, 17303.

S29. Z. Jiang, M. Li, T. Yan and T. Fang, *Appl. Surf. Sci.*, 2014, **315**, 16.

S30. S. Meng, E. G. Wang and S. Gao, *Phys. Rev. B*, 2004, **69**, 195404.

S31. A. A. Phatak, W. N. Delgass, F. H. Ribeiro and W. F. Schneider, *J. Phys. Chem. C*, 2009, **113**, 7269.

S32. R. Liu, *Comput. Theor. Chem.*, 2013, **1019**, 141.

S33. P. Wynblatt and R. C. Ku, *Surf. Sci.*, 1977, **65**, 511.

S34. M. Orlik and Z. Galus, *Electrochemistry of Gold*, Wiley-VCH, 2007,

S35. K. Fitzner, Q. Guo, J. Wang and O. J. Kleppa, *J. Alloys Compd.*, 1999, **291**, 190.

S36. V. A. Safonov, M. A. Choba, Yu. D. Seropegin and E. N. Lubnin, *Russ. J. Electrochem.*, 2006, **42**, 861 (*Elektrokhimiya*, 2006, **42**, 957).

S37. R. A. Manzhos, A. G. Krivenko, S. V. Doronin, M. A. Choba and V. A. Safonov, *J. Electroanal. Chem.*, 2013, **704**, 175.